SLAC-PUB-16402

RADIATION DOSE MEASUREMENTS FOR HIGH-INTENSITY LASER INTERACTIONS WITH SOLID TARGETS AT SLAC

T. Liang[1,2]*, J. Bauer[1], M. Cimeno[1], A. Ferrari[3], E. Galtier[1], E. Granados[1], H. J. Lee[1], J. Liu[1], B. Nagler[1], A. Prinz[1], S. Rokni[1], H. Tran[1], M. Woods[1]
[1]SLAC National Accelerator Laboratory, Menlo Park, CA USA
[2]Georgia Institute of Technology, Atlanta, GA USA
[3]HZDR Institute of Radiation Physics, Dresden, Germany

A systematic study of photon and neutron radiation doses generated in high-intensity laser-solid interactions is underway at SLAC National Accelerator Laboratory. These laser-solid experiments are being performed using a 25 TW (up to 1 J in 40 fs) femtosecond pulsed Ti:sapphire laser at the Linac Coherent Light Source's (LCLS) Matter in Extreme Conditions (MEC) facility. Radiation measurements were performed with passive and active detectors deployed at various locations inside and outside the target chamber. Results from radiation dose measurements for laser-solid experiments at SLAC MEC in 2014 with peak intensity between 10^{18} to 7.1×10^{19} W/cm^2 are presented.

INTRODUCTION

In recent years, the number and use of high power multi-terawatt and petawatt lasers to explore laser-matter interaction in research facilities has rapidly increased around the world. They are used to study matter under extreme conditions(1), to produce energetic beams of protons and/or electrons(2,3), or to generate forward-directed betatron X-rays(4,5).

This paper focuses on four radiation measurements performed during high-intensity laser shots on solid foils at SLAC National Accelerator Laboratory's Matter in Extreme Conditions (MEC) facility in 2014. The interaction of a high-intensity laser with a solid creates a thin plasma layer on the surface of the target and accelerates the electrons in the plasma to tens of MeV in energy(6,7). These "hot" electrons will interact with the laser target and the target chamber and generate bremsstrahlung(8,9). This mixed field of electrons and photons is a source of ionizing radiation and can create a radiation hazard for personnel unless sufficient radiological controls are implemented. A variety of active and passive detectors were deployed to measure the radiation doses generated from laser-solid interactions for 25 TW laser commissioning experiments at MEC in 2014.

MEC 25 TW LASER

For experiments in 2014, SLAC MEC utilized a Ti:sapphire short pulse laser system with wavelength of 0.8 μm, 1 J pulse energy, and 40 fs pulse width (FWHM). This provided a laser beam with a peak power of 25 TW to deliver intense light pulses onto solid targets. An off-axis parabolic (OAP) mirror focused the MEC laser beam to micrometer spot sizes to achieve laser intensities between 10^{16}–10^{20} W/cm^2. A target rastering system ensured each laser shot interacts with fresh target material at a laser repetition rate of 1 Hz.

Laser scientists performed a characterization of the high-intensity laser's beam parameters for each laser-solid experiment at MEC. The pulse energy was measured both before and after the compressor with a Coherent J50 50M-IR sensor and a Coherent LabMax-TOP meter†. The pulse duration was measured twice with two separate instruments, a Coherent single-shot autocorrelator (SSA) and an APE LX Spider autocorrelator‡, before and after each experiment. A charge-coupled device (CCD) camera, such as the Admiec OPAL-1000§, imaged the laser beam and determined the spot size. Figure 1 shows an image of a typical laser beam with a Gaussian-like profile achieved during laser-solid experiments at MEC.

Table 1 provides the laser beam parameters from the four laser-solid experiments at MEC in 2014. MEC achieved laser intensities up to 7.1×10^{19} W/cm^2. The uncertainty in achieved intensity is calculated to be about 38% for the February experiment and 20% for the July–August experiments. The hot electron temperature T_h is derived from laser parameters and characterizes the energy of the hot electrons generated from laser-solid interactions. Further details on T_h and

*Corresponding author: tliang6@slac.stanford.edu

† Coherent Inc., 5100 Patrick Henry Drive, Santa Clara, California 95054, USA

‡ APE Angewandte Physik und Elektronik GmbH, Plauener Strasse 163-165 Haus N, 1305 Berlin, Germany.

§ Adimec Electronic Imaging, Inc., 245 North Street, Stoneham, Massachusetts 02180, USA.

SLAC National Accelerator Laboratory, 2575 Sand Hill Road, Menlo Park, CA 94025
This material is based upon work supported by the U.S. Department of Energy, Office of Science, Office of Basic Energy Sciences, under Contract No. DE-AC02-76SF00515.

Table 1. MEC laser beam parameters from laser-solid experiments in 2014.

Experiment	Pulse energy (J)	Pulse width (fs)	Fraction of energy in peak	Peak power (TW)	$1/e^2$ spot size (μm × μm)	Peak intensity (W/cm^2)	T_h (MeV)
Feb-2014	1.0	70	0.19	2.8	13×8	1.8×10^{18}	0.18
Jul-2014	0.7	50	0.77	10.7	37×19	1.0×10^{18}	0.11
Aug-2014	0.7	50	0.44	6.1	9×5	1.0×10^{19}	0.71
Sep-2014	0.5	50	0.63	6.3	3×2	7.1×10^{19}	2.5

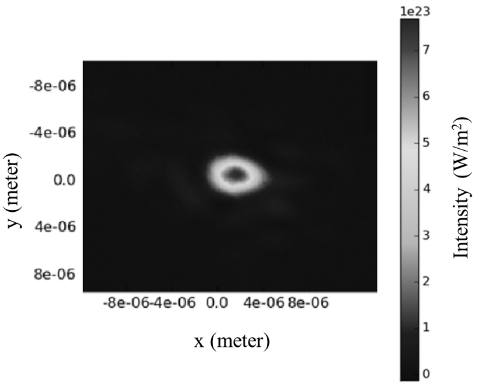

Figure 1. Laser beam intensity profile from the September 2014 laser-solid experiment at MEC, 7.1×10^{19} W/cm^2.

the radiation dose yield generated from hot electrons will be described in the next section.

SLAC RADIATION PROTECTION MODEL

The temperature T_h (or energy) of the hot electrons generated from laser-solid interactions is a crucial parameter to estimate the bremsstrahlung photon dose yield, and T_h is calculated from laser beam parameters. The value of T_h also determines how "hard" the hot electron energy and bremsstrahlung spectra is, which impacts the laser-generated ionizing radiation hazard.

Hot electron temperature and energy distribution

At lower laser intensities, inverse bremsstrahlung and resonance absorption are the dominant mechanisms for producing hot electrons. Meyerhofer *et al.* provides the scaling in Equation 1 to calculate the hot electron temperature T_h in MeV from the normalized laser intensity $I\lambda^2$(10).

$$T_h = 6 \times 10^{-8} (I\lambda^2)^{0.33} \tag{1}$$

At higher laser intensities, the ponderomotive force is the primary electron heating mechanism, and it is defined as the force that a dipole experiences in an oscillating electromagnetic field. For laser-plasma interaction, the electrons in the plasma experience the oscillating electric field of the incident laser pulse and gain energy. Equation 2 calculates the hot electron temperature T_h based on the ponderomotive force for $I\lambda^2 > 1.6 \times 10^{17}$ W μm^2/cm^2. The $m_e c^2$ term is the electron rest mass of 0.511 MeV(11–13).

$$T_h = m_e c^2 \left(-1.0 + \sqrt{1.0 + \frac{\mathrm{I}\lambda^2}{1.37 \times 10^{18}}} \right) \tag{2}$$

It is straightforward to calculate T_h from the laser beam parameters provided in Table 1 and with λ = 0.8 μm. The value of T_h can easily reach the MeV energy range as laser intensity increases. The values of T_h for the experiments in 2014 are shown in Table 1 and range from 0.18 MeV at 1.8×10^{18} W/cm^2 up to 2.5 MeV at 7.1×10^{19} W/cm^2.

Depending on the laser intensity, the distribution of the hot electrons generated from laser-solid interactions is often described as either a Maxwellian or relativistic Maxwellian distribution(14,15). Equations 3 and 4 provide the two distributions used by SLAC in characterizing the hot electron spectra.

$$N_e \propto E^{1/2}\, \mathrm{e}^{-E/T_h} \text{ for } I \leq 10^{19} \text{ W/cm}^2 \tag{3}$$

$$N_e \propto E^2\, \mathrm{e}^{-E/T_h} \text{ for } I > 10^{19} \text{ W/cm}^2 \tag{4}$$

For $I > 10^{19}$ W/cm^2, the average energy of the relativistic Maxwellian spectrum is $3T_h$, and electron energies in the tail portion of the hot electron spectrum can easily reach tens of MeV. The bremsstrahlung photons generated from MeV electrons can pose a challenge for a high power laser facility unless proper radiation shielding and controls are in place to mitigate the dose to personnel in the vicinity.

Dose equivalent from bremsstrahlung photons

Estimation of the bremsstrahlung dose (from hot electrons) is crucial in performing dose mitigation and establishing controls for high power laser experiments. Monte Carlo codes such as FLUKA can calculate the dose equivalent from a known hot electron source term

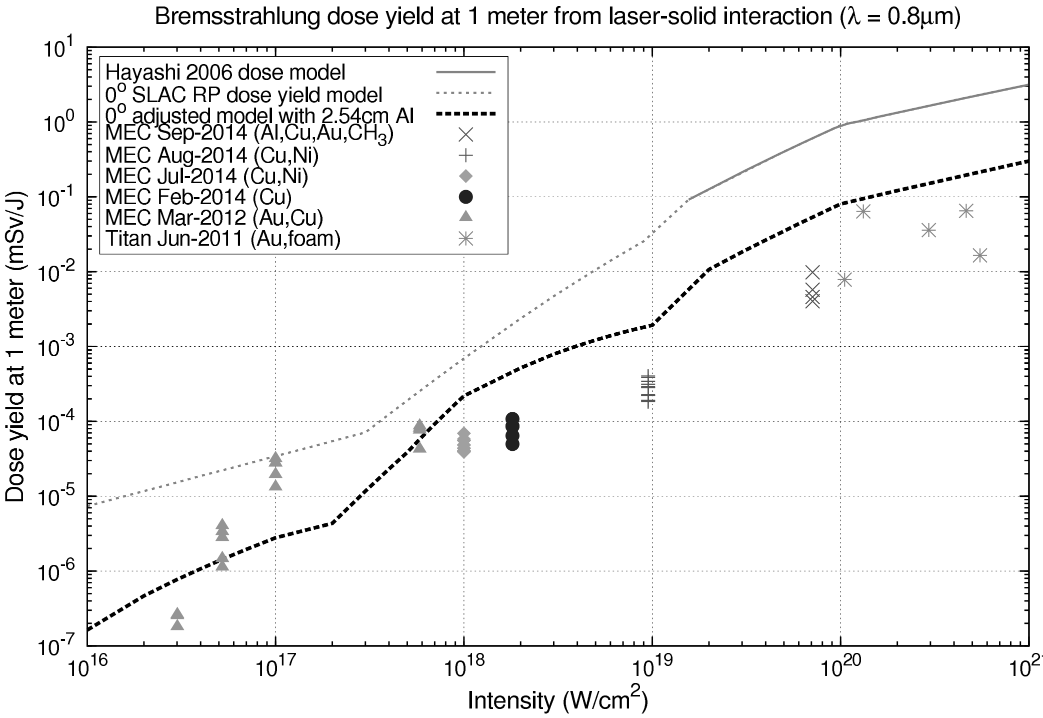

Figure 2. SLAC RP models for dose yield at 1 meter plotted with measured photon dose yield data from laser-solid experiments ($\lambda = 0.8\mu m$). The types of targets used during each laser-solid experiment are indicated in the legend. SLAC's adjusted RP model is scaled down to better reflect measurement data (see text description) and also includes an attenuation factor for 2.54 cm Al. Not all the dose yield points were measured in the 0° direction.

with a distribution described in Equations 3 and 4 and characterized by T_h in Equations 2. However, a simple empirical formula based on laser parameters and T_h can provide a quick estimate.

$$H_x \approx 1.8 \times \left(1.10 \times \frac{\alpha}{R^2}\right) T_h^2 \text{ for } T_h < 3 \text{ MeV} \quad (5)$$

$$H_x \approx 1.8 \times \left(3.32 \times \frac{\alpha}{R^2}\right) T_h \text{ for } T_h \geq 3 \text{ MeV} \quad (6)$$

Hayashi *et al.* established a dose yield model for estimating the 0° forward dose equivalent generated from a high power laser interacting with a thick solid target for $I\lambda^2$ = 10^{19}–10^{21} W μm^2/cm^2 or about T_h = 1–13 MeV(16). Equations 5 and 6 show the dose yield formulas proposed by Hayashi *et al.*, where α is the laser energy to electron energy conversion efficiency, and R is the distance from the laser-solid interaction point in cm. The dose yield parameter H_x is the dose equivalent (Sv) generated per joule (J) of laser energy in the 0° laser forward direction.

The SLAC radiation protection (RP) model expanded the dose model by Hayashi *et al.* to include laser intensities down to 10^{16} W/cm^2 with T_h calculated from Equations 1 and 2(17), and with the laser conversion efficiency α taken from work by Key *et al.* to be 30% for $I \leq 10^{19}$ W/cm^2 and 50% for $I > 10^{19}$ W/cm^2(18).

Figure 2 shows the SLAC RP 0° dose yield model at 1 meter as a function of intensity with λ = 0.8 μm. Also shown in Figure 2 are the maximum dose yields from several laser-solid experiments at SLAC's MEC and also one at Lawrence Livermore National Laboratory's (LLNL) Titan. The data points are collected from measurements at angles around the target chamber, not exclusively in the 0° direction.

The SLAC RP model overestimates the dose yield by when compared to the measurement data for laser intensities at 10^{18} W/cm^2 and above. Therefore, the dose yield model was scaled down by a factor of $1/10$ for laser intensities $\geq 10^{19}$ W/cm^2 and ramped down continuously from 10^{19} to 10^{18} W/cm^2 to better fit the measurement data. Attenuation factors for 2.54 cm Al are also applied to the adjusted model to take into account the shielding effect of the target chamber wall.

This adjusted model is not a perfect fit to the measurement data, but it provides a conservative and more realistic estimate of the radiation hazard generated from laser-solid experiments than the Hayashi dose model. SLAC currently uses the adjusted model to determine which radiological controls or shielding are needed to mitigate the dose to personnel.

MEC RADIATION DOSE MEASUREMENTS

A combination of passive and active detectors inside and around the outside of the MEC target chamber measured the radiation dose and dose equivalent generated from laser-solid interactions for different laser intensities. The target chamber is composed of aluminum, has a wall thickness between 2 to 6.4 cm, a radius of about 1 meter, and is pumped down to vacuum during high-intensity laser shots on target. Passive detectors measured the integrated dose (mGy) or dose equivalent (μSv) over a series of many laser shots on target, while active detectors provided dose equivalent rate (μSv/h) measurements in real-time during laser shots on target. Spectrometers were also used in an attempt to characterize the hot electron energy spectra. The results from the spectrometer measurements are not detailed here and will be discussed in a future publication. Table 2 provides a comprehensive list of the solid foils and their thicknesses that were used at targets during the laser-solid experiments at MEC in 2014.

Table 2. MEC laser shots and target description.

Intensity (W/cm^2)	Target material	Thickness (μm)	Number of laser shots
1.8×10^{18}	Cu	100	540
1.0×10^{18}	Cu+Kapton	5+30	550
	Ni	15	275
	Cu	100	655
1.0×10^{19}	Cu	100	340
	Ni	15	220
7.1×10^{19}	Al	15 & 10	70 & 66
	Au	5	22
	Cu	5	26
	CH_3	4 & 2.5	6 & 37

Dose inside target chamber

Small 1 cm $\times$ 1 cm passive (non-electronic) nanoDot* dosimeters from Landauer were used inside the MEC target chamber during laser-solid experiments for different target types and laser intensities. The nanoDot dosimeters were deployed at 30 cm distances radially around the laser-target interaction point and measured the dose in mGy from a mixed field of hot electrons and bremsstrahlung photons.

* LANDAUER, 2 Science Road, Glenwood, Illinois 60425, USA.

Figure 3 shows the dose measured by nanoDots for laser intensities 1.8×10^{18} and 10^{18} W/cm^2. The laser-target interaction point is at the center of the radial plot, and the laser axis is shown on each plot. The dose has been normalized to the number of laser shots delivered onto the solid target during each run. The dose profiles indicate that the mixed electron and photon fields generated from laser-solid interactions are emitted primarily in the forward and backward laser axis directions.

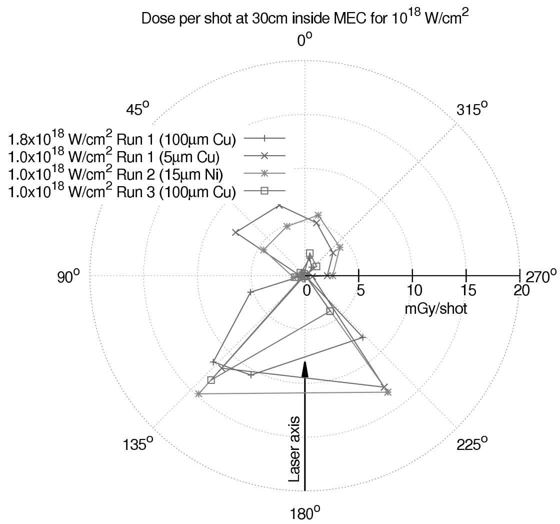

Figure 3. Dose per shot at 30 cm inside the target chamber for 10^{18} W/cm^2. The nanoDot at about 225° was blocked before run 3 (100 μm Cu) by an Al shield that was inserted to protect the OAP mirror.

The doses measured in the backward laser direction agree well with a maximum of about 15 mGy/shot. In contrast, the doses measured in the forward laser axis direction suggest a dependence on target thickness. The nanoDots in the forward direction measured less dose during shots on 100 μm copper than during shots on the thinner 5 μm copper and 15 μm nickel. Because the hot electron temperature is about 100–200 keV at 10^{18} W/cm^2 (from Equation 2), the self-shielding effect of the thicker 100 μm copper attenuates a large fraction of the hot electrons emitted in the forward direction.

Figures 4 and 5 show the radial dose profiles for two other laser-solid experiments at MEC for laser intensities of 10^{19} and 7.1×10^{19} W/cm^2. Looking at Figures 3–5, an increase in laser intensity leads to an increase in dose per shot generated inside the target chamber, as expected. Furthermore, the dose profiles become more forward peaked with increasing laser intensity. At 10^{19} W/cm^2, the dose is slightly forward peaked up to around 12 mGy/shot, and then at 7.1×10^{19} W/cm^2, the dose per shot is sharply forward

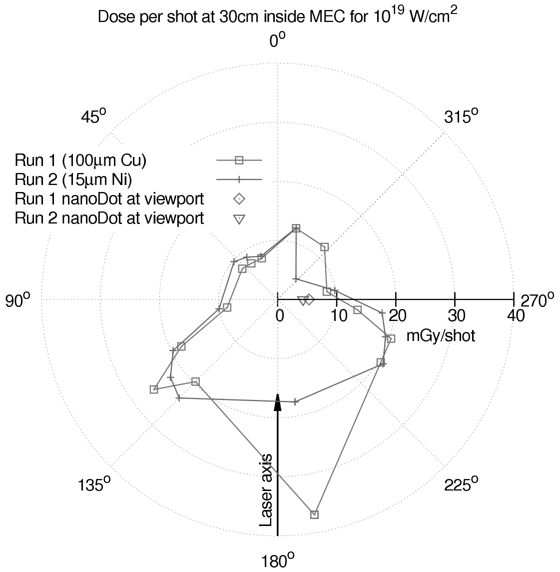

Figure 4. Dose per shot at 30 cm inside the target chamber for 10^{19} W/cm^2. A nanoDot was deployed outside the target chamber at a very thin diamond view port during each run, and the dose per shot was normalized to a distance of 30 cm.

peaked up to 45 mGy/shot. The shape and magnitude of the dose profiles depend on the laser intensity and the target thickness.

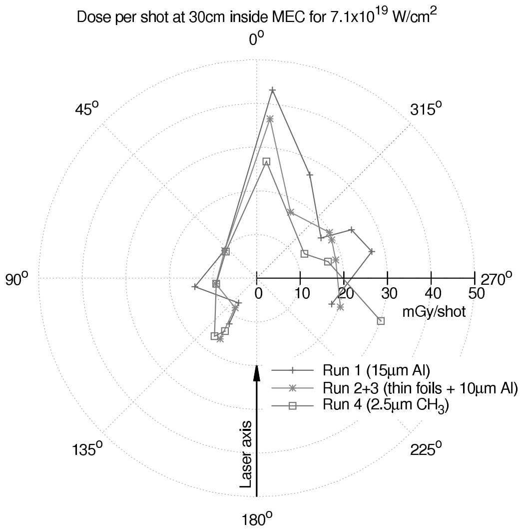

Figure 5. Dose per shot at 30 cm inside the target chamber for 7.1×10^{19} W/cm^2.

Photon dose outside target chamber

Hot electrons generated from laser-solid interactions will interact with the target material and the chamber walls to generated a bremsstrahlung photon field. Victoreen 451P† ion chambers were positioned at different angles around the outside of the MEC target chamber and recorded the ambient photon dose equivalent, H*(10), rate as μSv/h in real-time. For the remainder of this discussion, ambient dose equivalent rate will be referred to as simply dose rate.

The aluminum MEC target chamber is shaped like an octagon with a radius of about 1 meter. The octagonal target chamber has eight access doors along the "sides" and eight flanges (location of view ports) at the "corners". The chamber's doors are about 6.4 cm thick Al, and the flanges are about 2 cm thick Al.

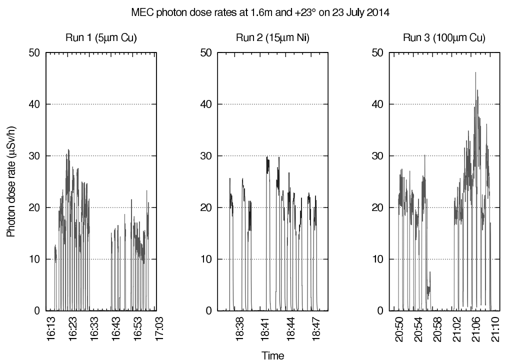

Figure 6. Photon dose rates measured by Victoreen 451P ion chamber at $r = 1.3$ m and $\theta = +23^\circ$ at MEC during July 2014 for 10^{18} W/cm^2.

The ion chambers were deployed in the forward and backward laser axis directions and at view ports if they were available. Ion chambers were also deployed at increasing radial distances to observe the drop in dose rate over distance. Figure 6 presents an example of the photon dose rates measured by a Victoreen 451P ion chamber from the July 2014 laser-matter experiment at MEC. The ion chamber's dose rates over time agree well between about 20–40 μSv/h for three different solid targets and also demonstrate good shot by shot stability of the laser intensity while operating at 1 Hz repetition rate. Figures 7–9 show the maximum photon dose rates measured at MEC for laser shots on solid targets from 10^{18} to 7.1×10^{20} W/cm^2. The dose rates have not been normalized and are shown "as measured."

† Fluke Biomedical, 6045 Cochran Road, Cleveland, Ohio 44139, USA.

July 2014 at MEC, 10^{18} W/cm^2

In Figure 7 for 10^{18} W/cm^2, the photon dose rates measured at the two view ports (or flanges) at 23° in the forward and backward laser axis directions agree well, and the same is evident at the chamber's doors at 0° and 45°. The photon dose rates of 30–50 μSv/h at the chamber's flanges are consistently higher by about a factor of 10 than the 4–5 μSv/h at the chamber doors. As a reminder, the aluminum target chamber doors are 6.4 cm thick, and the flanges are 2 cm thick. The Victoreen 451P ion chambers located at the doors measured less photon dose than the ones at the flanges due to aluminum attenuation.

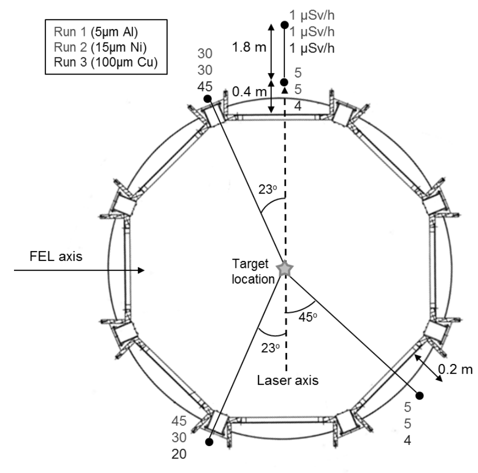

Figure 7. Maximum photon dose rates during each run at MEC during July 2014 for 10^{18} W/cm^2.

The two ion chambers located in the 0° forward direction measured about 5 μSv/h and 1 μSv/h at 1.4 m and 3.2 m distances from the laser-target interaction point, respectively, and the dose rate at 3.2 m is lower than at 1.4 m by a factor of $1/5$. This behavior at 10^{18} W/cm^2 operation suggests the photon dose falls off as $1/r^2$ and originates from the center of the target chamber whereas hot electrons interact with the solid target and generate bremsstrahlung.

Dependence on material type (copper or nickel) and target thickness has negligible effect on the measured bremsstrahlung dose rates outside the target chamber for 10^{18} W/cm^2 laser-solid experiments, and the photon dose rates at every location were within about a factor of 2 between runs.

August 2014 at MEC, 10^{19} W/cm^2

Figure 8 shows the maximum photon dose rates measured by ion chambers at MEC for two runs during a 10^{19} W/cm^2 laser-solid experiment. As expected, the photon dose rates for 10^{19} W/cm^2 are higher than for 10^{18} W/cm^2 (shown earlier in Figure 7) and do not scale linearly with laser intensity.

At 10^{19} W/cm^2, the photon dose rates generated from laser shots on 100 μm Cu are consistently higher within about a factor of 2 at all locations than from shots on 15 μm Ni. Since the Cu (Z = 29) and Ni (Z = 28) targets have similar mass densities, the higher photon dose rate measured for Cu may be because the Cu target is a little more than six times thicker than the Ni target, such that hot electrons produced from laser-solid interactions simply interact with more material and generate more bremsstrahlung in the 100 μm Cu target than in the 15 μm Ni target.

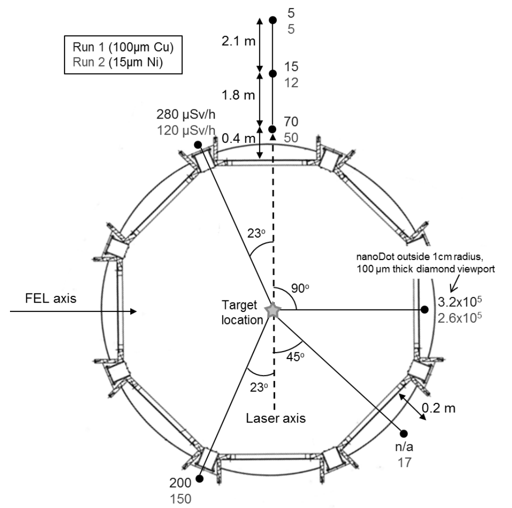

Figure 8. Maximum photon dose rates during each run at MEC during August 2014 for 10^{19} W/cm^2.

The photon dose rates are similar at the flanges at 23° in the forward and backward directions, and they are also consistently higher than the dose rates at the chamber's doors at 0° and 45°. Again, the difference in aluminum thickness between the flanges (2 cm) and the doors (6.4 cm) account for the difference in photon dose rates due to attenuation. In the 0° laser forward direction, the photon dose rates for both runs fall off with distance as $1/r^2$.

Also indicated in Figure 8 is a measurement made by a nanoDot dosimeter outside a small diamond view port with direct line of sight to the laser-target interaction location. The diamond view port was 100 μm thick with a radius of 1 cm and was located at 90° from the laser axis. Since the total number of shots and the laser repetition rate are known parameters, the integrated dose measured by the passive nanoDot dosimeter can be converted into a dose rate. The diamond view port dose rates are at least three orders of magnitude greater than what was measured around the aluminum chamber. Because 100 μm of diamond provides little to no shielding, measurements at the diamond view port represent the dose rate (from electrons and photons) at 1 meter if no shielding is present.

The diamond view port's nanoDot measurement can also be normalized to the total laser shots in a run and to a distance of 30 cm to obtain dose per shot inside the target chamber. The now normalized dose per shot at 30 cm agrees well within a factor of 2 to the nanoDot measurements inside the target chamber that were shown earlier in Figure 4.

September 2014 at MEC, 7.1×10^{19} W/cm^2

Radiation dose measurements in September 2014 at MEC were performed concurrent with another high power laser experiment at 7.1×10^{19} W/cm^2. To mitigate the radiation hazard to personnel, two 2.54 cm thick tungsten alloy (70% and 93%) shields were deployed in the forward and backward laser axis directions. Victoreen 451P ion chambers were positioned around the target chamber and on the roof, but the tungsten shielding blocked the ion chamber in the forward direction of the laser at 6°. The shielding did not affect the other ion chambers. Figure 9 shows the maximum photon dose rates measured by the ion chambers during runs 1–4 at MEC for 7.1×10^{19} W/cm^2.

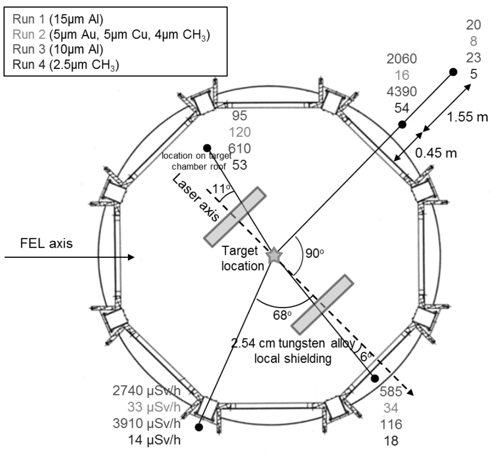

Figure 9. Maximum photon dose rates during each run at MEC during September 2014 for 7.1×10^{19} W/cm^2.

The MEC laser delivered continuous shots at 1 Hz onto the solid aluminum targets during runs 1 and 3. The ion chambers at 90° and 68° measured very high photon dose rates of 2,060 and 2,740 μSv/h during run 1, and dose rates of 4,390 and 3,910 μSv/h during run 3. The ion chamber located at 6° in the laser forward direction measured 585 and 116 μSv/h even though it was shielded by the 2.54 cm tungsten.

Runs 2 and 4 during the September 2014 laser-solid experiment did not utilize the MEC laser's continuous 1 Hz repetition rate. Instead, the laser system delivered single laser shots (frequency separated by up to one or more minutes) onto the solid targets. The ion chambers did not respond well for shot-by-shot detection, and their dose rate readings under-responded during runs 2 and 4 compared to runs 1 and 3. For example, the ion chambers at 90° and 68° measured 16 and 33 μSv/h during run 2 and 54 and 14 μSv/h during run 4, while they measured in the thousands of μSv/h during runs 1 and 3. The ion chambers also measured about an order of magnitude less dose rate during runs 2 and 4 in the laser forward direction at 6° even with the 2.54 cm tungsten alloy shielding.

The ion chamber deployed on the roof of the chamber measured a maximum dose rate of 610 μSv/h, which occurred during continuous laser shots on 10 μm Al. Unlike the other locations around the chamber, the roof did not measure significantly less dose during runs 2 and 4.

Photon dose measured by passive detectors at MEC

RADOS RAD-60‡ electronic dosimeters and Arrow-Tech Model 2§ (range of 0–20 μSv) pocket ion chambers or PICs were also deployed around the outside of the target chamber during laser-solid experiments at MEC. These passive instruments measured the integrated ambient dose equivalent from all shots onto the solid target during a run.

The integrated ambient doses were normalized to the total number of laser shots on target and the laser repetition rate and compared to measurements made by the active Victoreen 451P ion chambers. Measurements from passive dosimeters and active ion chambers were found to be in good agreement (especially between the 0–20 μSv PICs and the ion chambers) when enough laser shots were taken on target to generate an accumulated dose. The RAD-60 electronic dosimeters began to under-respond compared to the PICs at laser intensities greater than 10^{19} W/cm^2.

Neutron dose at MEC

Polyethylene-moderated BF_3 tubes (designed in-house at SLAC) were deployed around the target chamber and

‡ Mirion Technologies (MGP) Inc., 5000 Highlands Parkway, Suite 150, Smyrna, Georgia 30082, USA.

§ Arrow-Tech Inc., 417 Main Ave W, Rolla, North Dakota 58367, USA.

measured the neutron fluence generated from laser-solid experiments at MEC. Neutrons are generated primarily from photonuclear (γ, n) interactions when high energy bremsstrahlung from hot electrons interact with the target material or the chamber walls.

The BF_3 detectors are calibrated with an 11 GBq PuBe neutron source and compared to the ambient neutron dose equivalent rate measured by a Model 5085 Meridian* neutron survey meter. A conversion factor is derived for each BF_3 detector to convert the neutron fluence to ambient dose equivalent. A typical conversion factor for a BF_3 is about 10^5 counts per μSv.

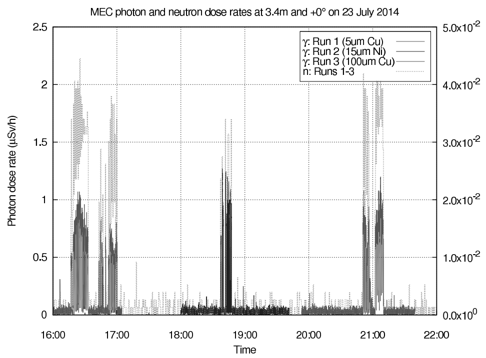

Figure 10. Photon and neutron dose rates at MEC during July 2014 for 10^{18} W/cm^2. Please note the different scales for photons and neutrons.

Figure 10 shows an example of the measurements performed by both a BF_3 and a Victoreen 451P ion chamber. The plot shows that whenever the ion chambers measured photons, the BF_3 also measured neutrons at the same time. In addition, the instruments showed that a neutron dose rate of about 3–4×10^{-2} μSv/h was consistently generated from a photon dose rate of about 1 μSv/h.

The ambient neutron dose equivalent rates (μSv/h) measured by BF_3 detectors can be normalized into a neutron dose yield (μSv/J) since laser beam parameters such as laser repetition rate and pulse energy are well characterized. Figure 11 shows the neutron dose yields normalized to a distance of 1 meter from laser-solid interactions. The data suggests the neutron dose yield increases with laser intensity, which is expected. The prompt neutron dose rate is small compared to the prompt photon dose rates, but at higher intensities, it has the potential to activate equipment inside and around the target chamber.

* Health Physics Instruments, 330 D South Kellogg Ave., Goleta, California 93117, USA.

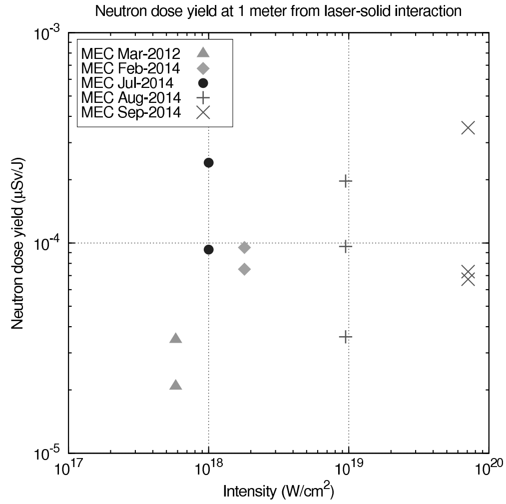

Figure 11. Neutron dose yield at 1 meter from laser-solid experiments at MEC.

DISCUSSION

As presented earlier in Figure 2, radiation measurements by SLAC have covered a wide range of laser intensities from 10^{16}–10^{21} W/cm^2. The data points in the figure represent the maximum dose yields at 1 meter measured by a combination of active and passive detectors during each experiment.

Studies by Bauer *et al.* have detailed elsewhere the radiation dose measurements performed at LLNL's Titan laser facility in 2011 (between 10^{20}–10^{21} W/cm^2) and at SLAC's MEC in 2012 (between 10^{16}–10^{18} W/cm^2). The dose yields from these two laser-solid experiments agree well with the trend of increasing dose yield as a function of laser intensity, and the measurements below 10^{18} W/cm^2 agree especially well with the RP models. Bauer *et al.* also observed at Titan that electronic-based detectors around the target chamber (i.e. ion chambers and RAD-60) did not respond during laser shots on solid target, and only passive PICs responded properly[19,20].

The dose yields from laser-solid experiments in 2014 show good agreement within a factor of 2 to 3 when compared to the adjusted model[21]. The differences between the measurement data and the dose yield models may be due to uncertainties behind the derivation of the model. The model's laser-to-electron conversion efficiency α of 30–50% may be too optimistic. A single hot electron temperature parameter T_h may not be enough to fully characterize the time-dependent fluctuating temperature of the laser-induced plasma.

The transition of the hot electron spectrum from a Maxwellian distribution to a "hotter" relativistic Maxwellian at 10^{19} W/cm^2 (Equations 3 and 4) may actually occur at a higher laser intensity. For example, a shift in the hot electron spectrum from a relativistic Maxwellian distribution to just Maxwellian would significantly affect the attenuation factor by 2.54 cm Al that is applied to the dose yield model. If the transition to a relativistic Maxwellian distribution occurs at 10^{20} W/cm^2, the dose yield model at 10^{19} W/cm^2 will be lower because attenuation by 2.54 cm Al at 10^{19} W/cm^2 will be higher.

The measurements at 7.1×10^{19} W/cm^2 are about a factor of $1/3$ below the adjusted model. It should be noted that tungsten local shielding blocked the instruments in the forward laser direction during this experiment, so the dose yields shown in the figure are from other angles. Since the RP model estimates the dose yield in the $0°$ forward direction, it is expected that the detectors at other angles will measure less than the model due to the very forward-directed nature of the dose yield at high laser intensities.

SUMMARY

The radiation protection department at SLAC and colleagues at MEC have measured ionizing radiation generated from the interaction of a high-intensity laser with solid targets between 10^{16}–10^{21} W/cm^2. The laser beam parameters are well characterized, and sustained laser shots on different solid targets were delivered. A combination of passive and active detectors were used to measure the dose yield in mSv/J outside the target chamber, and the SLAC RP dose yield model was adjusted to better reflect the measurement data. Inside the target chamber, passive nanoDot dosimeters measured very high doses per shot up to 45 mGy/shot in the forward direction of the laser at 7.1×10^{19} W/cm^2, and showed that the radial dose levels increase and become more forward peaked with increasing laser intensity. Outside the target chamber, active Victoreen 451P ion chambers and passive RAD-60 dosimeters and 0–20 μSv PICs characterized the ambient photon dose equivalent at various angles and recorded the data in real-time. BF_3 detectors also measured ambient neutron dose equivalent rates that coincided with ion chambers' measurements. SLAC's radiation protection program utilizes the adjusted dose yield model to design radiation shielding and establish controls at the Matter in Extreme Conditions (MEC) laser facility in order to mitigate the radiation hazard to its personnel, and the

ACKNOWLEDGMENT

The author wishes to thank the staff of SLAC from radiation protection and LCLS and also N. Hertel of Georgia Institute of Technology.

The work presented here was supported by the United States Department of Energy under contract number DE-AC02-76SF00515.

REFERENCES

1. Fletcher, L. B. *et al. Ultrabright X-ray laser scattering for dynamic warm dense matter physics*. Nat. Photonics **9**, 274–279 (2015).
2. Leemans, W. P. *et al. GeV electron beams from a centimetre-scale accelerator*. Nat. Phys. **2**, 696-699 (2006).
3. Fourmaux, S. *et al. Investigation of laser-driven proton acceleration using ultra-short, ultra-intense laser pulses*. Phys. Plasmas **20**, 013110 (2013).
4. Albert, F. *et al. Angular Dependence of Betatron X-ray Spectra from a Laser-Wakefield Accelerator*. Phys. Rev. Lett. **111**, 235004 (2013).
5. Chen, L. M. *et al. Bright betatron X-ray radiation from a laser-driven-clustering gas target*. Scientific Reports **3**, 1–5 (2013).
6. Tajima, T. and Dawson, J. M. *et al. Laser electron accelerator*. Phys. Rev. Lett. **43**, 267–270 (1979).
7. Wilks, S. C. and Kruer, W. L. *Absorption of Ultrashort, Ultra-Intense Laser Light by Solids and Overdense Plasmas*. IEEE J. Quantum Electron. **33**, 1954–1968 (1997).
8. Guo, T. *et al. Generation of hard x rays by ultrafast terawatt lasers*. Rev. Sci. Instr. **72**, 41–47 (2001).
9. Chen, L. M. *et al. Study of hard x-ray emission from intense femtosecond Ti:sapphire laser-solid target interactions*. Phys. Plasmas **11**, 4439–4445 (2004).
10. Meyerhofer, D. *et al. Resonance absorption in high-intensity contrast, picosecond laser-plasma interactions*. Phys. Fluids B **5**, 2584–2588 (1993).
11. Chen, H. *et al. Hot electron energy distributions from ultraintense laser solid interactions*. Phys. Plasmas **16**, 020705 (2009).
12. Mulser, P. and Bauer, D. *High Power Laser-Matter Interactions*. Springer Berlin Heidelberg, 416 p, (2010).
13. Kluge, T. *et al. Electron Temperature Scaling in Laser Interaction with Solids*. Phys. Rev. Lett. **107**, 205003 (2011).
14. Borne, F. *et al. Radiation Protection for an Ultra-high Intensity Laser*. Radiat. Prot. Dosimetry **102**, 61–70 (2002).
15. Ledingham, K. W. D. *et al. Photonuclear Physics when a Multiterawatt Laser Pulse Interacts with Solid Targets*. Phys. Rev. Lett. **84**, 899–902 (2000).
16. Hayashi, Y. *et al. Estimation of photon dose generated by a short pulse high power laser*. Radiat. Prot. Dosimetry **121**, 99–107 (2006).
17. Qiu, R. *et al. Analysis and mitigation of x-ray hazard generated from high intensity laser-target interactions*. SLAC Publication SLAC PUB–14351, 1–9 (2011).

18. Key, M. *et al. Hot eletron production and heating by hot electrons in fast ignitor research*. Phys. Plasmas **5**, 1966–1972 (1998).
19. Bauer, J. *et al. High Intensity Laser Induced Radiation Measurements at LLNL*. SLAC Radiation Physics Note RP–11–11, 1–16 (2011).
20. Bauer, J. *et al. Measurements of Ionizing Radiation Doses Induced by High Irradiance Laser on Targets in LCLS MEC Instrument*. SLAC Publication SLAC PUB–15889, 1–39 (2013).
21. Liang, T. *et al. Measurements of high-intensity laser induced ionising radiation at SLAC*. Shielding Aspects of Accelerators, Targets and Irradiation Facilities SATIF-12 Workshop Proceedings , 40–53 (2015)